Investigation into Atomic Diffusion at the Interface During Extrusion Welding of Magnesium and Magnesium Alloys

Bai, Shengwen; Fang, Gang; Jiang, Bin; Zhou, Jie

Citation (APA)
Bai, S., Fang, G., Jiang, B., & Zhou, J. (2021). Investigation into Atomic Diffusion at the Interface During Extrusion Welding of Magnesium and Magnesium Alloys. *Metallurgical and Materials Transactions A: Physical Metallurgy and Materials Science*, *52*(9), 4222-4233. https://doi.org/10.1007/s11661-021-06381-8

Important note
To cite this publication, please use the final published version (if applicable).
Please check the document version above.

Investigation into atomic diffusion at the interface during extrusion welding of magnesium and magnesium alloys

Shengwen Bai[1, 2], Gang Fang[2, *], Bin Jiang[1, 3] Jie Zhou[4]

[1] State Key Laboratory of Mechanical Transmissions, College of Materials Science and Engineering, Chongqing University, Chongqing, 400044, China
[2] State Key Laboratory of Tribology, Department of Mechanical Engineering, Tsinghua University, Beijing 100084, China
[3] Chongqing Academy of Science and Technology, Chongqing, 401123, China
[4] Department of Biomechanical Engineering, Delft University of Technology, Mekelweg 2, 2628 CD Delft, The Netherlands

*Corresponding author, Gang Fang: Tel: +86-10-6278 2694, E-mail: fangg@tsinghua.edu.cn

Abstract

This research was aimed to reveal atomic diffusion across the bonding interface through the extrusion-welding experiments of dissimilar materials, namely pure magnesium and Mg-Al-Zn-RE alloy. A special tooling setup used to simulate weld seam formation during extrusion through a porthole die was designed for this model study. To deform the metal streams symmetrically and create a sound weld seam, the extrusion-welding experiments from sandwich-structured billets were carried out. Chemical analysis of diffused atoms in the welding region was performed by electron probe micro-analysis. The results confirmed that atomic diffusion indeed occurred across the interface during extrusion. The gradients in element concentration, local stresses, and hydrostatic pressure were considered to be the necessary conditions for extensive atomic diffusion to occur. Atomic diffusion was significantly enhanced by raising extrusion temperature. The analysis of the stress and hydrostatic pressure distributions in the welding region provided new insights into the mechanisms of weld seam formation during the extrusion of light metals.

Keywords: magnesium; extrusion; solid-state bonding; weld seam; atomic diffusion

1 Introduction

Tubes, pipes and hollow profiles of light metals are particularly attractive for applications in automobiles and aerospace due to their lightweight advantage [1]. The vast majority of hollow products made of magnesium, aluminum and their alloys are efficiently manufactured by means of hot extrusion through porthole dies [2]. During

extrusion, a preheated billet is forced to be divided into several metal streams, while being pushed to flow into and then through a porthole die. The neighboring metal streams become reunited and welded in the solid state, under a high pressure, at a high temperature and in a short time frame inside the welding chamber of the porthole die. Then, the welded metal streams flow as a whole through the clearance between the die orifice and the mandrel to form a hollow product with longitudinal weld seams in the extrusion direction along its entire length. In other words, in this way of manufacturing, longitudinal weld seams are inevitably present in the products. Obviously, defective weld seams and even imperfect bonding even at the micro scale will have negative effects on the mechanical performance of such products. Liu et al. [3], for example, found that fracture occurred along the weld seams, when the tube of AZ31 magnesium alloy extruded through a pothole die was sectioned. To prevent extruded products from unexpected failure, product designers and extrusion die designers are expected to find a way to avoid unfavorable loading conditions in the weld seam region, when the extruded product is in use. However, in many cases, this is impossible. Therefore, a fundamental understanding of extrusion welding is of vital importance for the design of extruded products and extrusion dies, for the selection of extrusion process parameters, and for the achievement of the desired mechanical properties of the extruded products at the weld seams, comparable to those far away from the weld seams.

So far, a lot of research has been performed to gain this understanding. It is now commonly understood that extrusion welding belongs to solid-state bonding occurring at a temperature below the melting point of the metal without liquid metal involved [4]. This distinguishes itself from the welding commonly applied to fuse metal pieces together, with the melting of the base material involved in the joining process. It is also understood that for solid-state bonding to take place, metal pieces must be brought together within the range of inter-atomic forces. The two metal pieces to be welded in the solid state must have absolutely clean and smooth surfaces. Kazakov [5] demonstrated that solid-state bonding could take place at an elevated temperature even without external pressure, if they were in conforming contact with each other. In practice, however, asperities at the sub-micro level are always present on the real surfaces of metal pieces, even with high surface finish achieved by precision machining. Besides, light metals are highly reactive and have a great affinity to oxygen to form a thin protective film of oxide instantly after exposure to an oxygen-rich atmosphere. As a result, the surfaces of magnesium and aluminum alloys are always covered by an oxide film. The presence of surface asperities and oxide film hinder the formation of inter-atomic forces, because in this case it is difficult to achieve atom-scale contact between two metal pieces. Therefore, in order to achieve sound solid-state bonding, high pressure and temperature are both necessary to crash surface asperities, break up the oxide films, soften the material for easy deformation and speed up atomic diffusion [6]. Solid-state bonding can be divided into three stages. At the first stage, only the tips of surface asperities meet each other, and many

micro-voids are formed at the interface. The actual contact area at the interface is much smaller than the nominal contact area. Shimizu et al. [7] demonstrated that the oxide films prevented the metal surfaces from effective contact at the initial stage. At the second stage, the height of surface asperities decreases along with increasing plastic deformation, resulting in the shrinkage of micro-voids at the interface. At the same time, the hard, brittle oxide films are broken up as plastic deformation progresses, contributing to the formation of inter-atomic forces, due to more exposed fresh metal surfaces [8]. At the last stage, the micro-voids at the interface under high pressure and at an elevated temperature further shrink and become completely closed. Meanwhile, the broken-up oxide films are redistributed in the bonding region. Some of the oxides may become decomposed in the matrix material, if the holding time is long enough. Xie et al. [9], for example, found that the oxides at the bonding interface of the 316LN stainless steel became decomposed and a particle precipitation zone was formed around the weld seam after holding at 1200 °C (1473 K) for 24 h.

As aforementioned, the micro-voids at the interface and oxide films are the dominant barriers to solid-state bonding. During extrusion welding, only the shrinkage of voids must be taken into consideration, while the effect of oxide films on solid-state bonding can be largely ignored. This is because metal streams are created while the metal enters the portholes so that these metal streams have fresh surfaces and become bonded in a closed welding chamber inside the porthole die, before being oxidized. Yu et al. [10] confirmed that no oxides could be observed at the weld seam, when the porthole die with a deep welding chamber was employed during the extrusion of an Al-Mg-Si aluminum alloy to produce a hollow profile.

During solid-state bonding, mass transfer relies on atomic diffusion, while plastic deformation activates and enhances the diffusion mass transfer by speeding up the shrinkage of micro-voids at the interface. Chen et al. [11] established a mathematical model to estimate the individual contributions of plastic deformation and atomic diffusion to micro-void shrinkage during the diffusion bonding of zirconium-based bulk metallic glasses. The measured bonding strength was in agreement with the predicted results obtained from their mathematical model. Hill and Wallach [12] modeled the diffusion bonding of similar materials with grain boundary diffusion considered to be an additional contributor. In comparison with diffusion bonding, extrusion welding takes place in a short time frame, but with serve plastic deformation and high hydrostatic pressure involved. Clearly, plastic deformation plays a particularly important role in bringing about micro-void shrinkage. Bai et al. [13] demonstrated that the weld seam quality could be improved by increasing the strain at the interface. It was however not clear if atomic diffusion across the interface indeed occurred during extrusion welding and how atomic diffusion would influence the weld seam quality. Obviously, the answers to these research question would be of great help to understand the fundamental mechanisms of extrusion welding.

Element diffusion during the diffusion bonding of dissimilar metals have been extensively studied. Liu et al. [14], for example, investigated the inter-diffusion of

elements, i.e., magnesium and aluminum, during diffusion bonding of pure magnesium and the aluminum alloy 1060. Intermetallic compounds (IMCs), i.e., Al_3Mg_2 and $Mg_{17}Al_{12}$, were detected at the interface, and the depth of the zone where IMCs were present increased with lengthening holding time. Zhu et al. [15] simulated the diffusion of aluminum and magnesium atoms during diffusion bonding of the aluminum alloy 6061 and magnesium alloy AM50 by combining the methods of the CALculation of PHAse Diagrams (CALPHAD) and diffusion modeling. The formation and growth of a Mg-Al inter-diffusion layer (with the presence of the $Mg_{17}Al_{12}$ and Al_3Mg_2 phases) were revealed, based on the simulated and measured results. In these studies, the diffusion model, based on Fick's second law, was used to describe the mass transfer around the interface and to estimate the concentration profiles of the elements adjacent to the bonded interface. Chen et al. [16] determined the diffusion coefficients of Ni in Cu and in the Ti-6Al-4V titanium alloy, based on the modeling and experimental results. Sun et al. [17] modified Fick's second law by taking the effects of strain and strain rate on the diffusion coefficient into consideration to account for solid-state bonding in hot-forming processes. The concentration profiles of Fe, Cr and Ni around the bonded interface between the plain carbon steel Q235 (equivalent to ASTM A36) and stainless steel 316L, predicted by the modified model, were in good agreement with the experimental results.

In the above cited studies, atomic diffusion during the diffusion bonding of dissimilar metals was revealed by using energy dispersive spectroscopy (EDS) and electron probe micro-analyzer (EPMA) [18]. However, the research on atomic diffusion across the weld seam formed during extrusion through a porthole die is scarce. It is important to note the distinct differences between the diffusion bonding and extrusion welding, although both take place in the solid state. Diffusion bonding of metals typically takes a long bonding time (several hours), allowing atomic diffusion across the interface into the substrates. By contrast, during extrusion welding, metal screams are bonded within a very short time frame (a few seconds) but exposed to severe plastic deformation and high hydrostatic pressure. It is therefore of particular interest to ascertain whether sufficient atomic diffusion indeed occurs at the extrusion welding interface.

In the case of the solid-state bonding of similar metals, it is difficult to ascertain atomic diffusion and to reveal the redistribution of elements adjacent to the interface experimentally. Zhang et al. [19], for example, characterized and analyzed the interface region with a void zone, a diffusion zone and a bonding zone at different time points of diffusion bonding by means of scanning electron microscopy (SEM) and EDS line scanning. They could only reveal the diffusion behavior at the void tip to ascertain the contribution of diffusion to void shrinkage. In the case of extrusion welding taking place inside a porthole die, it is inherently difficult to track and trace diffused atoms across the interface, because the same material from the same source (i.e., the billet) becomes welded inside the inaccessible welding chamber of the porthole die. One could only assume that atomic diffusion occurred during extrusion

welding and contributed to micro-void shrinkage. Based on this assumption, Yu et al. [20] established an extrusion-welding criterion and verified it by performing extrusion experiments. However, there have been no experimental studies ever performed to show and characterize atomic diffusion across the extrusion weld interface, although the evidence of its occurrence is badly need to support the assumption.

The present work was intended to fill this knowledge gap. It concerned a model study, aimed to reveal atomic diffusion during the extrusion welding of magnesium-based materials. Pure magnesium and an Mg-Al-Zn-RE alloy were configured in a sandwich form for the extrusion-welding experiments, with which atomic diffusion across the interface could be captured. To this end, a dedicated extrusion tooling set up was designed. The extrusion-welding experiments were carried out at various billet temperatures and stem speeds. In addition, finite element (FE) simulations of extrusion were carried out to quantify the thermal and mechanical parameters inside the welding chamber, i.e., temperature, hydrostatic pressure and equivalent stress, which were experimentally immeasurable. The element distributions adjacent to the bonded interface were revealed by using EPMA. The effects of the extrusion process parameters on atomic diffusion were analyzed to aid in gaining a fundamental understanding of the role of atomic diffusion in weld seam formation during extrusion in relation to the local thermomechanical conditions.

2 Experiments and FE simulation

2.1 Materials

High-purity magnesium and an Mg-Al-Zn-RE alloy were used as the experimental materials in the extrusion-welding experiments so as to allow the identification of atomic diffusion across the solid-state bonding interface. The billets of pure magnesium and the Mg-Al-Zn-RE alloy were supplied by Changchun Institute of Applied Chemistry. Their chemical compositions determined by inductively coupled plasma emission spectroscopy are given in Table I. The impurities, e.g., Al, Zn, Mn, La and Gd, in pure magnesium were all less than 0.01%. In the Mg-Al-Zn-RE alloy, however, the content of Al reached 8.399%. Therefore, aluminum was taken as a tracking and tracing element, whose redistribution adjacent to the interface between pure magnesium and the Mg-Al-Zn-RE alloy was supposed to reflect the extent of atomic diffusion occurring during extrusion welding.

Prior to extrusion welding, the as-cast Mg-Al-Zn-RE alloy was solid-solution treated at 420 °C (693 K) for 24 h, followed by water quenching, in order to dissolve most of second-phase particles and thus maximize the difference in solute concentration between the two α-Mg matrices on both sides of the interface. The microstructures of the solid-solution treated Mg-Al-Zn-RE alloy and the as-cast pure magnesium are shown in Fig. 1. The average grain size of the Mg-Al-Zn-RE alloy

was 165 $\pm$ 5 μm [21], while the grain sizes of pure magnesium were much larger. Only one complete grain of pure magnesium could be observed in the field of view at the lowest magnification (50) of the optical microscope used.
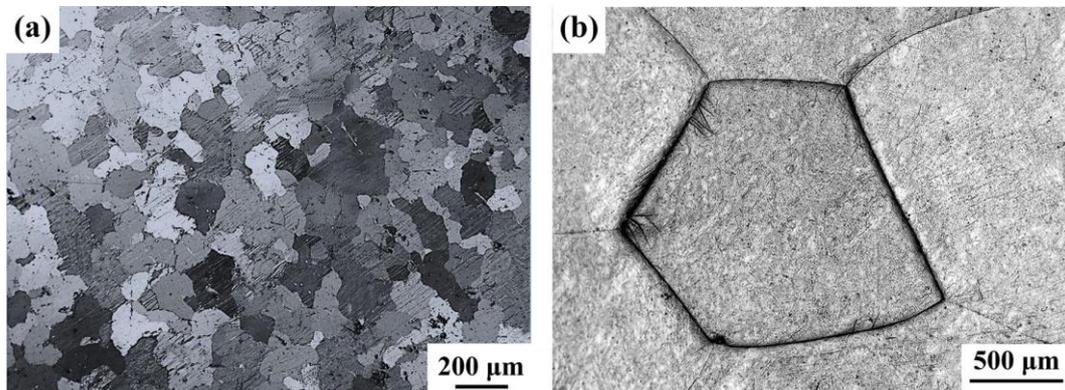

Fig. 1. Grain structures of (a) the solid-solution treated Mg-Al-Zn-RE alloy, reprinted from [21], and (b) the as-cast pure magnesium.

Table I. Chemical compositions of pure magnesium and Mg-Al-Zn-RE alloy (wt.%)

Element	Al	Zn	Mn	La	Gd	Mg
Pure magnesium	0.009	0.003	0.006	<0.0005	<0.0005	Bal.
Mg-Al-Zn-RE alloy	**8.399**	0.524	0.162	1.099	0.382	Bal.

2.2 Extrusion welding tooling setup

An extrusion-welding tooling setup, including a stem, a die set, a container and a supporting structure, was tailor-designed to simulate extrusion welding physically (Fig. 2). In order to be able to take the extrusion-welded materials out after extrusion welding, a die set with a conical outer surface at an angle of 3° was designed in such a way that it could be symmetrically split into two halves (i.e., split die 1 and split die 2 in Fig. 2a). The die set was inserted into the container. The die set and the container together were mounted on a supporting structure (Fig. 2a). During the extrusion-welding experiments, the two halves of the die set were forced to stick together tightly under a high extrusion load and within the constraints of the container. After extrusion welding, the die set was pushed out of the container by applying a small force opposite to the extrusion direction, and then the extrusion-welded materials could be taken out.

Considering the fact that the flow stress of pure magnesium was lower than that of the Mg-Al-Zn-RE alloy at the same extrusion condition, to create sound weld seams, synchronous deformation of these two materials would have to be maintained. A sandwich configuration of the billet composed of one pure magnesium layer sandwiched by two thicker layers of the Mg-Al-Zn-RE alloy was designed so as to maintain symmetrical outflow of the bonded materials in the form of a plate from the die orifice (Fig. 2a, b and c). As shown in Fig. 2f, the cross-section dimensions of the

pure magnesium layer and each of the two same magnesium alloy layers were 4×30 mm and 23×30 mm, respectively. Thus, the total cross-section dimensions of the sandwich-structured billet were 50×30 mm, which were the same as the sizes of the welding chamber inside the die set. The length of the sandwich-structured billet was 20 mm. The cross-section dimensions of the die orifice were 30×3 mm (Fig. 2e). The die orifice with a non-uniform bearing length and a trapezoidal bulge in the middle was designed to slow down the flow of pure magnesium and to maintain balanced metal flow (Figs. 2d and 2e). During the extrusion-welding experiments, the sandwich-structured billet was extruded into a plate at an extrusion ratio of 16.67. Two weld seams were formed along the plate length in the extrusion direction (Fig. 2b).

Four heating rods inserted into the die set were used to heat the billet and die set to a pre-set temperature at a rate of 10 K/min. A hold time of 10 min was given. Sensors used to measure force and temperature (thermocouple) were integrated into the extrusion-welding tooling setup. Thermocouple I near the welding chamber was used to monitor the billet temperature and regulate the heating through a PID temperature controller. During extrusion welding, the temperature near the die orifice was measured by thermocouple II (Figs. 2c and 2e) and used for comparison with FE simulation results.
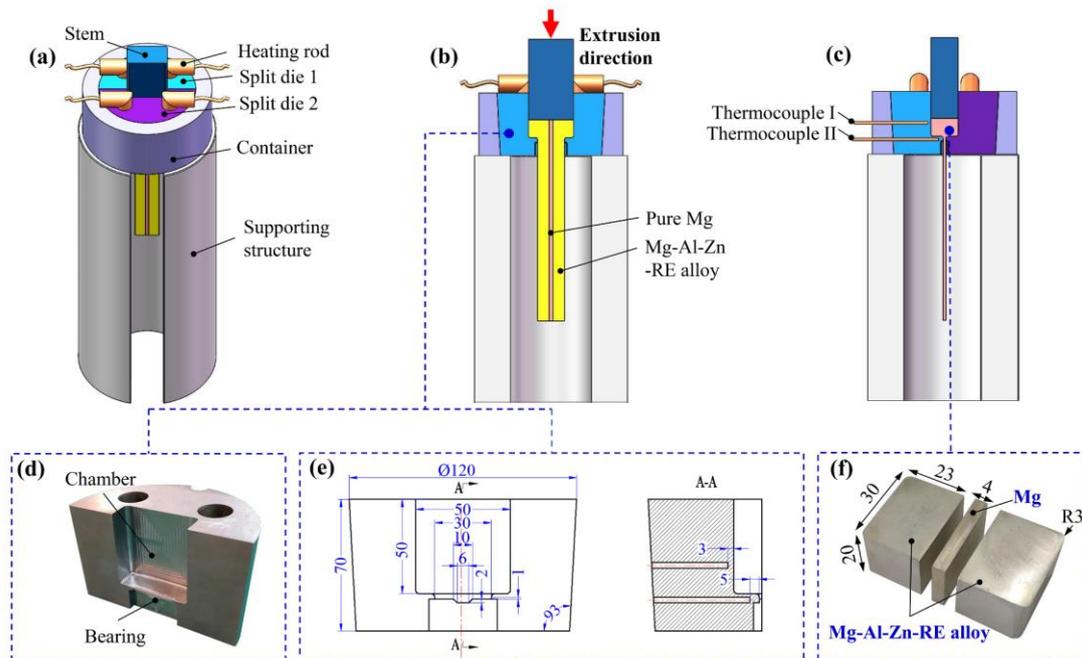

Fig. 2. Schematic of the extrusion-welding tooling setup: (a) oblique view, (b) front sectional view and (c) side sectional view, (d) die set, (e) dimensions of the die set, and (f) sandwich-structured billet with pure magnesium at the middle and the magnesium alloy on both sides.

2.3 Extrusion-welding experiments

The extrusion-welding experiments were conducted by using the dedicated tooling setup mounted on a hydraulic press with a load capacity of 2000 kN. Before extrusion welding, the surfaces of the sandwich-structured billet were mechanically polished to remove the oxide film and reduce roughness. The sandwich-structured billet was inserted into the chamber of the die set. Subsequently, the extrusion-welding experiments were performed at a stem speed of 0.2 mm/s and temperatures of 250 °C (523 K), 300 °C (573 K), 350 °C (623 K) and 400 °C (673 K), as well as at a temperature 350 °C (623 K) and at stem speeds of 1.0 and 2.0 mm/s, which fell into the ranges of temperatures and strain rates typically applied in the hot deformation of the AZ81-based alloy [22]. During extrusion welding under one condition, three billet components were solid-state bonded at a high temperature and under a high pressure in the welding chamber and subsequently extruded out of the die orifice in parallel. After extrusion, the die set together with the extruded plate was cooled by immersing them in water so as to freeze the microstructure and element distribution.

The microstructure in the welding region was characterized by using optical microscopy (OM, Zeiss Axio Scope A1). The distributions of solute element concentrations across the interface were analyzed using EPMA (JXA-8230). The scanning step size of EPMA was set to be 0.1 μm. Samples were prepared from the extruded plates by wire electro-discharge machining (Fig. 3). The samples for microstructural analysis were ground, mechanically polished and ultrasonically cleaned in alcohol. The OM samples were etched in an etchant composed of 60 ml absolute ethyl alcohol, 20 ml acetic acid, 15 ml deionized water and 5 ml nitric acid.
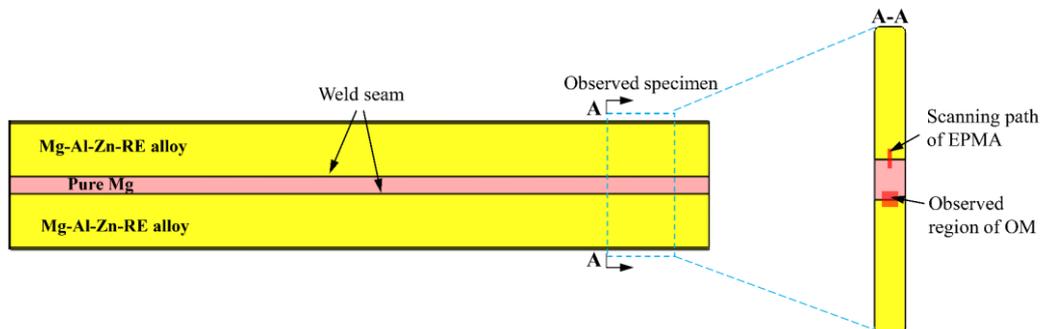

Fig. 3. Schematic of sampling from the extrusion-welded plate for structure and composition analysis.

2.4 Finite element simulations of extrusion

FE simulations of extrusion were performed by using the commercial software package DEFORM-3D to quantify the state variables during the extrusion process, i.e., temperature, stress and hydrostatic pressure along the welding path. It should be noted that the FE model only simulated the metal flow during extrusion, but not the

real welding process. In other words, the interfaces between pure magnesium and the Mg-Al-Zn-RE alloy in the FE model were regarded as general boundary contacts.

Fig. 4 shows the FE model, including the die, stem, and sandwich-structured billet. Since all the objects were symmetrical, only one-quarter of these objects were used for FE simulation. The die and stem were considered to be rigid, while the billet was assumed to be a rigid-plastic body. All the objects were meshed into tetrahedral elements. Heat transfer between the extrusion tooling and billet was allowed in the FE model. The thermal properties of the billet and tooling were as the same as those used in a previous study [21], in which the FE model was validated by performing extrusion experiments. The shear friction model with a friction coefficient of 1.0 was adopted between the tooling and billet [23]. The billet temperatures and stem speeds set in the FE simulations were the same as those used in the extrusion-welding experiments. The following constitutive models of the pure magnesium (Eq. 1) [24] and the Mg-Al-Zn-RE alloy (Eq. 2) [21] were used in the FE simulations.

$$\dot{\varepsilon} = 3.039 \times 10^{12} [\sinh(0.01\sigma)]^5 \exp\left(\frac{-135000}{RT}\right) \tag{1}$$

$$\dot{\varepsilon} = 2.319 \times 10^{10} [\sinh(1.72 \times 10^{-2}\sigma)]^{4.516} \exp\left(\frac{-141329}{RT}\right) \tag{2}$$
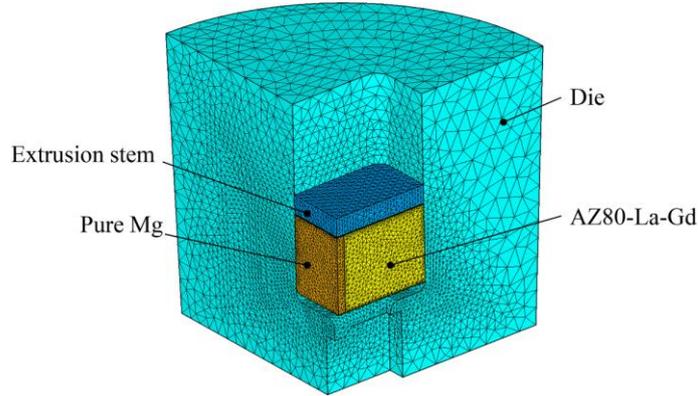

Fig. 4. One-quarter symmetrical FE model of the extrusion-welding process.

In these constitutive equations, $\dot{\varepsilon}$ is the strain rate, σ the equivalent stress, T the absolute temperature, and R the universal gas constant.

The FE model was verified through comparing the numerically simulated temperatures with the values measured by thermocouple II at the same spot near the die orifice. The result demonstrated that the simulated and experimentally temperatures agreed well with each other, indicating that FE model of extrusion was reliable in temperature calculation (Fig. 5).
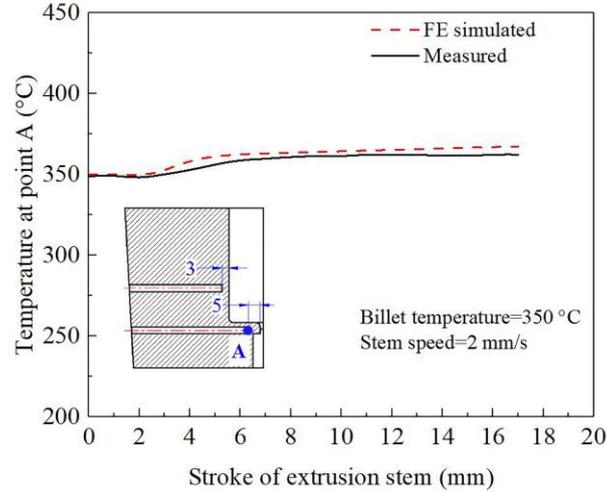
Fig. 5. Comparison between the measured and simulated temperatures near the die orifice.

3. Results and discussion

3.1 Microstructure evolution adjacent to the solid-state bonding interface

Fig. 6 shows an example of the extrusion-welded plate. It was composed of the pure magnesium in the middle and the Mg-Al-Zn-RE alloy on both sides. Two straight weld seams along the extrusion direction were formed at the interfaces between the pure magnesium and the Mg-Al-Zn-RE alloy. With respect to the extrudate shape and the locations of the two weld seams, the designed extrusion-welding tooling setup was confirmed to be able to serve the purpose of the extrusion-welding experiments.
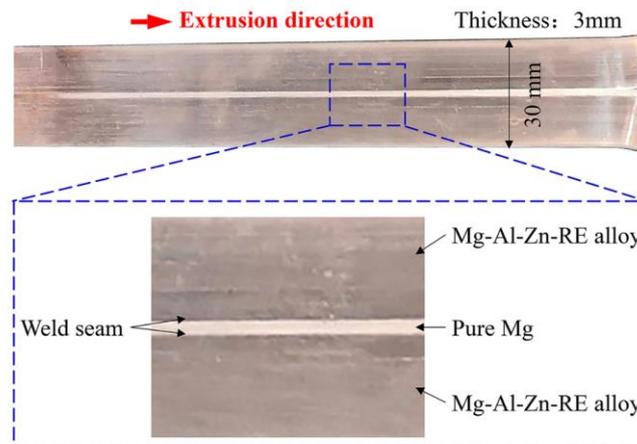

Fig. 6. Extrusion-welded plate composed of pure magnesium in the middle and the Mg-Al-Zn-RE alloy on both sides.

The microstructure characteristics near the interface were of critical importance for evaluating the quality of the extrusion weld seam. Fig. 7 shows the optical micrographs of the plate extruded at different billet temperatures (T_b) and stem speeds

(V_r). The observation region is near one of the solid-state bonding interfaces, as depicted in Fig. 3. No micron-scale voids were observable at the interface, indicating that the pure magnesium and Mg-Al-Zn-RE alloy were solid-state bonded well during the extrusion-welding experiments (Fig. 7). Since the different sensitivities of the two materials to the same etchant, only the grain boundaries of the Mg-Al-Zn-RE alloy were observed after etching under a specific condition. The weld seam could be clearly identified under the OM (Fig. 7). During extrusion welding, the grain sizes of the alloy decreased due to dynamical recrystallization (DRX). At a stem speed of 0.2 mm/s and a billet temperature of 250 °C (523 K), a partially dynamically recrystallized (un-DRX) grain structure was observed on the Mg-Al-Zn-RE alloy side (Fig. 7a). However, when billet temperature was raised to 300 °C (573 K) or higher, complete DRX occurred during extrusion welding. The DRX grain size increased with rising billet temperature. The average grain sizes of the Mg-Al-Zn-RE alloy were 2.6, 4.3 and 7.1 μm, when extrusion welding was performed at a stem speed of 0.2 mm/s and billet temperatures of 300 °C (573 K), 350 °C (623 K) and 400 °C (673 K), respectively (Figs. 7b, 7c and 7d). This trend could be attributed to the growth of DRX grains promoted by increasing temperature. With increasing stem speed from 0.2 to 1.0 and to 2.0 mm/s, the average grain sizes of the alloy rose from 4.3 to 5.6 and to 6.7 μm, respectively (Figs. 7c, 7e and 7f). On the one hand, a high strain rate corresponding to a high stem speed contributed to grain refinement, because of reduced time for grain growth. On the other hand, the real temperature of the material during extrusion welding increased with arising stem speed, promoting the growth of grains [20]. In the present study, it was observed that temperature increment played a more dominant role in the evolution of grain sizes, especially at a high stem speed, than the changes of stem speed.
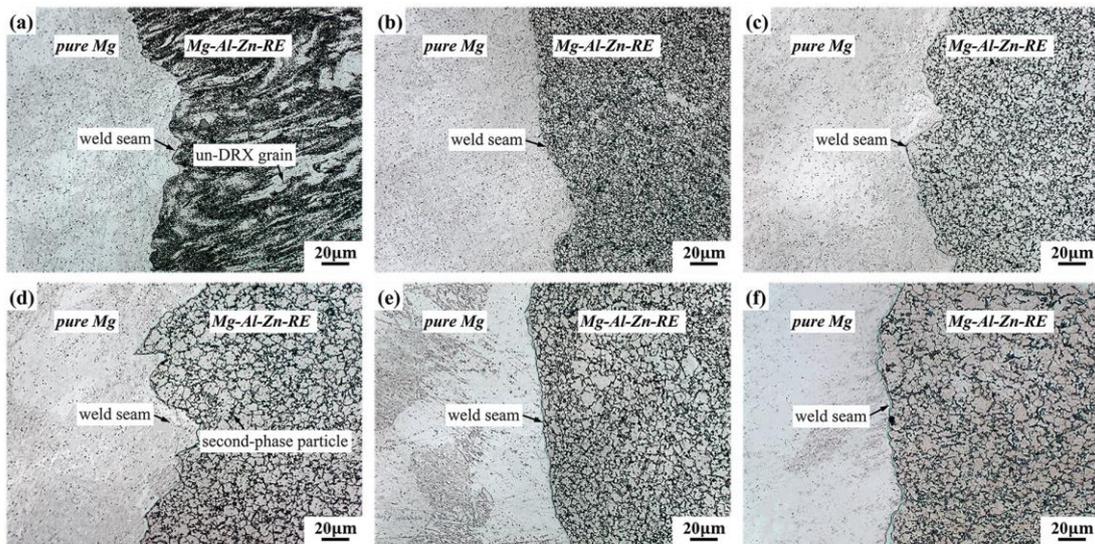

Fig. 7. Optical micrographs showing the grain structures around the weld seam in the plate extruded under different conditions: (a) T_b=250 °C (523K); V_r=0.2 mm/s, (b) T_b=300 °C (573 K);

11

V_r=0.2 mm/s, (c) T_b=350 °C (623 K); V_r=0.2 mm/s, (d) T_b=400 °C (673 K); V_r=0.2 mm/s, (e) T_b=350 °C (623 K); V_r=1.0 mm/s, and (f) T_b=350 °C (623 K); V_r=2.0 mm/s.

3.2 Atomic diffusion during extrusion welding

EPMA was performed to determine the distributions of the diffused atoms in the extrusion weld seam region on both sides of pure magnesium and the Mg-Al-Zn-RE alloy. Fig. 8a shows an EPMA scanning path over a length of 50 μm, perpendicular to the weld seam. The analysis was repeated twice at least for all the extrusion conditions to ensure that the results were reliable. At the welding interface, no new phase was visible under SEM. Fig. 8b depicts the distributions of magnesium and aluminum along the scanning path in the plate extruded at a billet temperature of 400 °C (673K) and stem speed of 0.2 mm/s. On the side of pure magnesium, aluminum was detected and its concentration reduced from the interface to the interior. On the other side of the weld seam, the concentration of aluminum increased from the interface to the interior until it reached the level in the Mg-Al-Zn-RE alloy. By contrast, the concentration of magnesium decreased from pure magnesium across the interface to the Mg-Al-Zn-RE alloy. The concentration profiles clearly indicated that atomic diffusion indeed occurred at the interface during extrusion welding, because the element concentrations changed gradually on both sides of the weld interface, rather than abruptly. On the side of the Mg-Al-Zn-RE alloy, some spikes and troughs appeared in the concentration profiles of aluminum and magnesium (Fig. 8b). This must have been due to the remaining second-phase particles in the as-solution-treated alloy and more importantly due to the newly precipitated second-phase particles containing aluminum, such as $Mg_{17}Al_{12}$, where the concentration of aluminum was raised and correspondingly the concentration of magnesium reduced, as compared to the α-Mg matrix. This was confirmed by the previous research, which showed increased fractions of the $Mg_{17}Al_{12}$ and $Al_{11}La_3$ phases in the Mg-Al-Zn-RE alloy after extrusion welding due to dynamic precipitation [21].
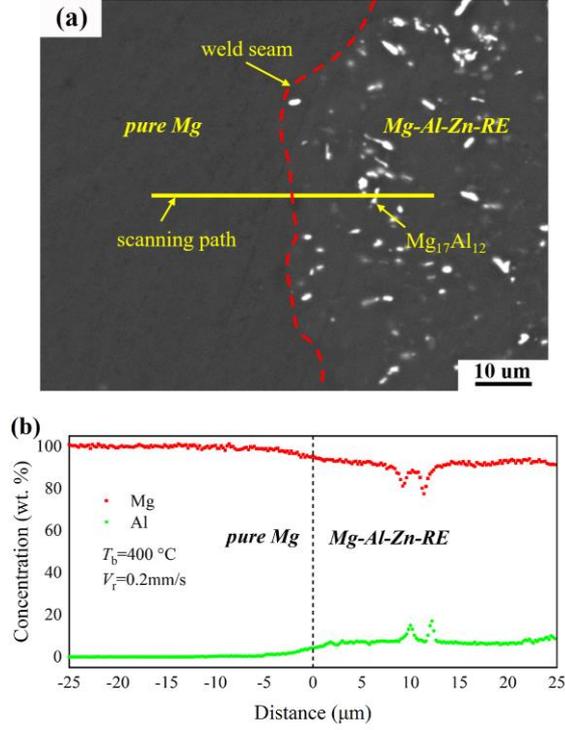
Fig. 8. (a) SEM micrograph of the extrusion-welding interface and (b) concentration profiles of magnesium and aluminum across the interface.

The extent of atomic diffusion from the bonding interface could be represented by the characteristic diffusion length L_d, which could be obtained from the non-linear regression of experimental data by using Fick's second law (Eq. 3) [25]:

$$\varphi = \frac{\varphi_1 + \varphi_2}{2} + \frac{\varphi_2 - \varphi_1}{2} \, \text{erf}\left(\frac{x}{0.5L_d}\right) \tag{3}$$

where φ is the element concentration along the scanning path of EPMA, and the parameters φ_1 and φ_2 are the initial element concentrations in pure magnesium and in the Mg-Al-Zn-RE alloy, respectively, before solid-state bonding. x represents the distance from the weld seam. Fig. 9 shows the fitted curve and measured aluminum concentration profile. At a billet temperature of 400 °C (673 K) and stem speed of 0.2 mm/s, the characteristic diffusion length L_d of aluminum was measured to be 10.2 ± 0.3 μm.

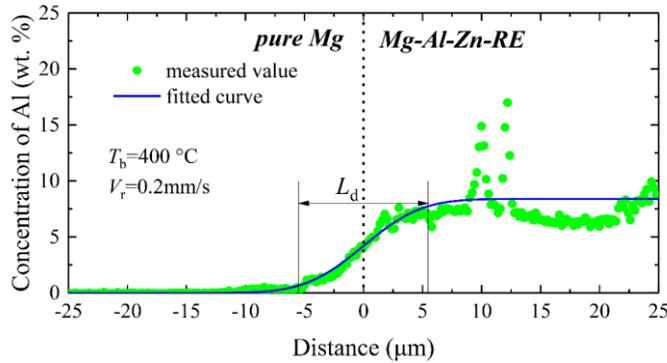Extrusion conditions, namely billet temperature and extrusion stem speed, significantly influenced the atomic diffusion length into the other side of the interface. Table II lists the L_d values of magnesium and aluminum at different extrusion conditions, together the exact extrusion temperatures (T_e) and welding times (t), predicted by the FE model. When the extrusion stem speed was 0.2 mm/s and the billet temperatures were 250 °C (523 K), 300 °C (573 K), 350 °C (623 K) and 400 °C (673 K), the L_d values of magnesium were 4.4 ± 0.3, 5.9 ± 0.7, 7.5 ± 0.5 and 10.5 ± 0.1 μm, respectively, and those of aluminum were 3.4 ± 0.2, 4.3 ± 0.4, 7.1 ± 0.6 and 10.2 ± 0.3 μm, respectively. Clearly, the L_d value increased with rising billet temperature, indicating that a higher billet temperature led to enhanced atomic diffusion over the weld seam. This is because the higher the temperature, the easier it is for atoms to jump from one site to another due to the higher energy, resulting in a greater diffusion length [25]. Moreover, the characteristic L_d values of magnesium were slightly greater than those of aluminum. Zhong and Zhao [26] found that the self-diffusion coefficient of magnesium was larger than the diffusion coefficient of aluminum in pure magnesium, which was consistent with the findings of the present study (Table II).

When the billet temperature was fixed at 350 °C (623 K), the L_d value decreased first and then increased with increasing stem speed. Taking aluminum as an example, L_d decreased from 7.1 ± 0.6 to 4.1 ± 0.4 μm, as the stem speed increased from 0.2 to 1.0 mm/s, and then it increased to 4.6 ± 0.5 μm when the stem speed increased further to 2.0 mm/s. On the one hand, the higher the stem speed, the shorter the welding time (t), which was not conducive to atomic diffusion. The corresponding welding times at extrusion stem speeds of 0.2, 1.0 and 2.0 mm/s were 89.5, 17.9 and 9.0 s, respectively. On the other hand, the actual extrusion temperature increased during the extrusion-welding process due to the heat generated from plastic deformation and severe friction, which had less time to dissipate [27]. When the billet temperature was 350 °C (623 K), the simulated extrusion temperature (T_e) increased from 360 °C (633 K) to 424 °C (697 K), as the stem speed increased from 0.2 to 2.0 mm/s. The large temperature rise at a high stem speed promoted atomic diffusion across the weld seam. Since the competition between the effects of welding time and temperature rise on atomic diffusion, the characteristic diffusion length L_d changed non-monotonically with increasing stem speed.

Table II. Characteristic diffusion lengths L_d of magnesium and aluminum during extrusion welding under different conditions.

Stem speed V_r (mm/s)	Welding time t (s)	Characteristic diffusion length L_d (μm)

Billet temperature T_b (°C)		Extrusion temperature T_e (°C)		Mg	Al
250 (523 K)		292 (565 K)		4.4±0.3	3.4±0.2
300 (573 K)	0.2	323 (596 K)	89.5	5.9±0.7	4.3±0.4
350 (623 K)		360 (633 K)		7.5±0.5	7.1±0.6
400 (673 K)		405 (678 K)		10.5±0.1	10.2±0.3
350 (623 K)	1.0	390 (663 K)	17.9	4.3±0.1	4.1±0.4
	2.0	424 (697 K)	9.0	5.1±0.2	4.6±0.5

3.3 Mechanism of atomic diffusion during extrusion welding

In the dedicated model study carried out, it was ascertained that atomic diffusion indeed occurred across the weld seam between pure magnesium and the Mg-Al-Zn-RE alloy. Fick's second law was utilized to predict the concentration distribution of aluminum across the weld seam [28].

$$\varphi = \frac{\varphi_1 + \varphi_2}{2} + \frac{\varphi_2 - \varphi_1}{2} \, \mathrm{erf}\left(\frac{x}{2\sqrt{\int_0^t D(T)dt}} \right) \tag{4}$$

where t is the welding time, and $D(T)$ the diffusion coefficient, which is a function of temperature T [29].

$$D(T) = D_0 \exp\left(\frac{-Q_d}{RT} \right) \tag{5}$$

where D_0 is the pre-exponential factor, Q_d the diffusion activation energy, T the absolute temperature, and R the universal gas constant (8.314 J/mol K). For the diffusion of aluminum into the magnesium matrix, the values of D_0 and Q_d are 6.25×10^7 µm²/s and 139.3 kJ/mol, respectively [30].

The temperature at the weld seam was extracted from the simulated results by the point tracing method in DEFORM and fed into Eqs. (4) and (5) to calculate the concentration profile of aluminum. Fig. 10 shows the calculated distribution of aluminum compared with the aluminum concentration profile measured by EPMA. Surprisingly, the calculated distribution was quite different from the measured values. At a billet temperature of 400 °C (673 K) and stem speed of 0.2 mm/s, for example, the calculated L_d was only 1.6 µm, being much smaller than the measured value (10.2 ± 0.3 µm). It indicated that atomic diffusion predicted by Fick's second law grossly underestimated atomic diffusion occurring during extrusion welding. The discrepancy was caused by the fact that in Fick's second law, i.e., Eq. (4), only element

concentration gradient was considered as the driving force of atomic diffusion. In fact, at the interface, in addition to the action of concentration gradient, hydrostatic pressure and stress are at play as well [31]. Due to the difference in flow stress between pure magnesium and the Mg-Al-Zn-RE alloy under the same extrusion condition, stress gradient and the hydrostatic pressure gradient perpendicular to the weld seam were both present. Figs. 11 and 12 show the simulated equivalent stress and hydrostatic pressure distributions, respectively, at a billet temperature of 400 °C (673 K) and stem speed of 0.2 mm/s. The data points along the paths A, B and C were extracted by using the point tracing method (Figs. 11b and 12b). Along the paths A, B and C, the equivalent stresses of pure magnesium near the weld seam were 29, 35 and 38 MPa, respectively while those of the Mg-Al-Zn-RE alloy were 47, 54 and 59 MPa, respectively (Fig. 11b). The hydrostatic pressures acting on the Mg-Al-Zn-RE alloy near the weld seam were also higher than those on pure magnesium (Fig. 12b). The atomic diffusion flux J across the weld seam of the two materials could be expressed by:

$$J = -D(T)(\nabla\varphi + k_1\nabla\sigma + k_2\nabla P_m) \tag{6}$$

where $\nabla\varphi$, $\nabla\sigma$ and ∇P_m represent the gradients of element concentration, stress and hydrostatic pressure, respectively. Parameters k_1 and k_2 are the factors that represent the individual effects of stress and hydrostatic pressure, respectively.
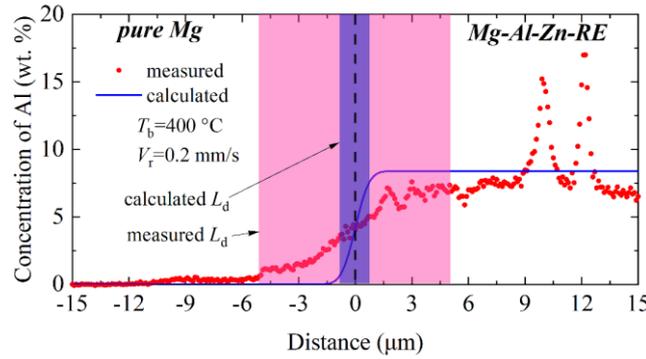

Fig. 10. Aluminum distribution calculated by applying Fick's second law, compared with the aluminum concentration profile measured by EPMA.
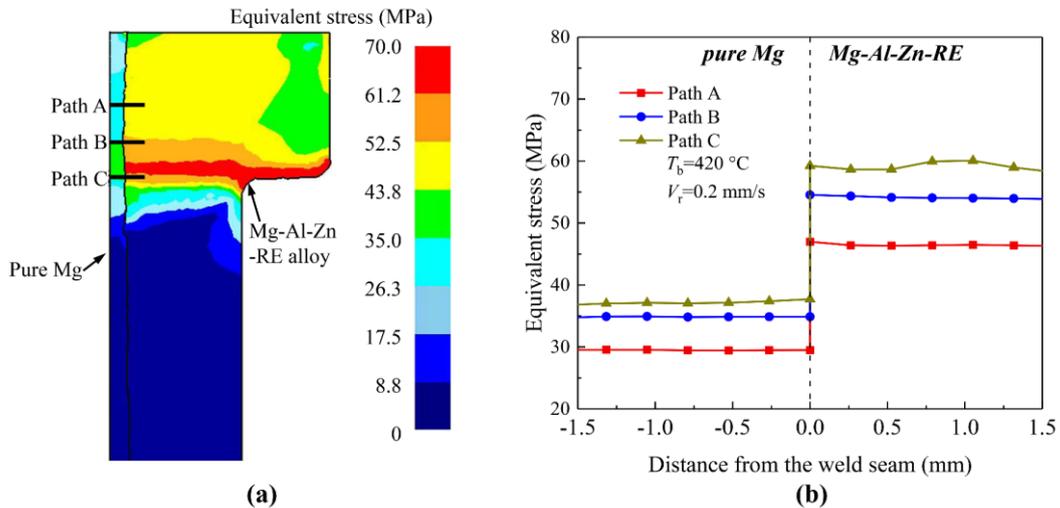

(a)　　　　　　　　　　　　(b)

Fig. 11. Distribution of the simulated equivalent stresses during extrusion welding (a) and the extracted equivalent stresses along the paths A, B and C (b).

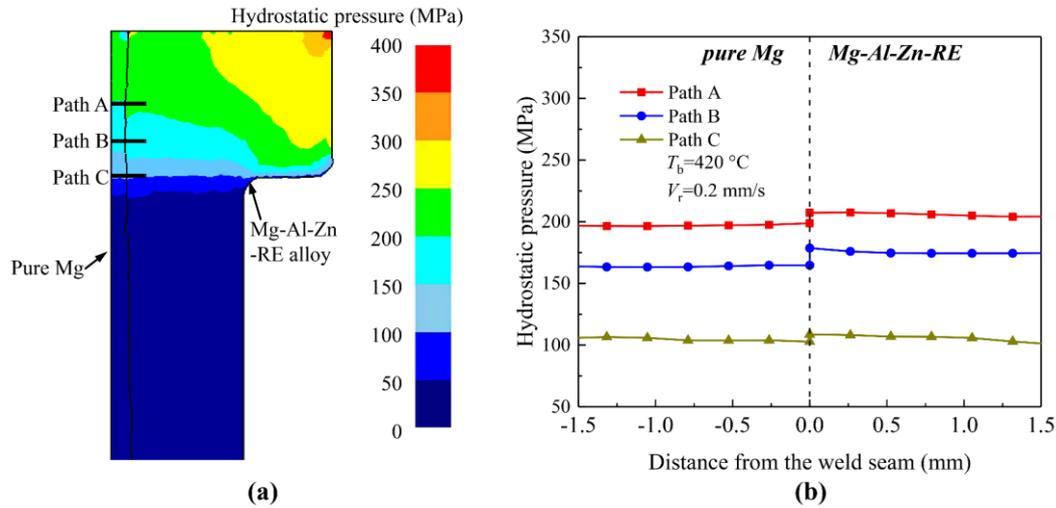**(a)**   **(b)**

Fig. 12. Distribution of the simulated hydrostatic pressures during extrusion welding (a) and the extracted hydrostatic pressures along the paths A, B and C (b).

Indeed, the internal driving force of atomic diffusion is the gradient of chemical activity. The extrusion welding of magnesium alloys is a complex thermomechanical process and it is practically impossible to quantify the chemical activity at the weld interface formed inside a porthole die. In the current study, the gradient of chemical activity near the welding interface is mainly affected by the gradient of element concentration, stress and hydrostatic pressure. The gradient of element concentration is determined by the billet materials. For example, the difference in aluminum concentration between the two sides of the welding interface (namely, pure magnesium and the Mg-Al-Zn-RE alloy) is as high as 8.4%. The gradients of stress and hydrostatic pressure near the welding interface also depend on the materials. In the current study, the stresses of pure magnesium alloy are consistently lower than those of the Mg-Al-Zn-RE alloy at the all chosen extrusion conditions (Fig. 11).

During the extrusion welding of pure magnesium and the Mg-Al-Zn-RE alloy, atomic diffusion across the weld seam occurred due to the gradients of element concentration, stress and hydrostatic pressure. The last two factors played an important role in promoting atomic diffusion. It may be inferred that, in the case of the extrusion welding of the same material, atomic diffusion would occur when hydrostatic pressure is present, even without element concentration gradient between the two sides of the weld seam. During extrusion through a porthole die to produce a hollow profile, metal streams of the same composition become welded at a high temperature and under a high hydrostatic pressure in the welding chamber. Micro-voids may remain at the interface due to surface asperities. These micro-voids influence the distribution of hydrostatic pressure in the welding region, resulting in the gradient of hydrostatic pressure. When a void is present at the interface, as illustrated in Fig. 13, in the region close to the void (i.e., region A), hydrostatic pressure is quite low, and, away from the void, it gradually increases. In the region far

away from the void (i.e., region B), hydrostatic pressure stays at a high level determined by the extrusion process parameters and die geometry and sizes. The gradient of hydrostatic pressure facilitates atomic diffusion to occur along the direction toward the interfacial void. This supports the assumption of Yu et al. [20] that atomic diffusion contributed to the shrinkage of voids during extrusion welding. Therefore, their extrusion-welding criterion including the diffusion coefficient (i.e., the J criterion) is an objective and valid one. Indeed, their experimental results indicated that the J criterion had a higher prediction accuracy than the "pressure-time" criterion (i.e., the Q criterion) and the "pressure-time-flow" criterion (i.e., the K criterion). It is now clear that, in addition to plastic deformation, atomic diffusion from the matrix to the voids at the interface, driven by the gradient of hydrostatic pressure, also contributed to mass transfer and promoted the shrinkage of interfacial voids during extrusion welding.
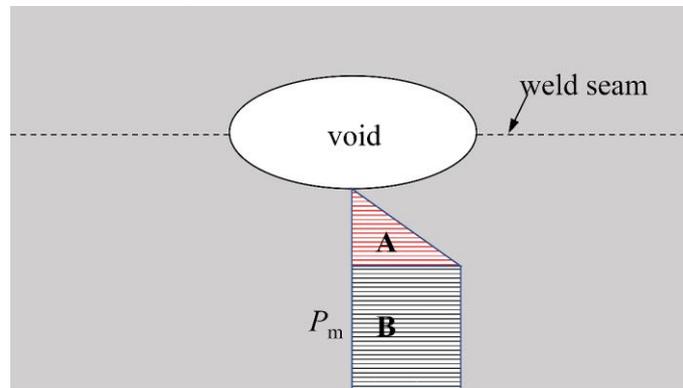

Fig. 13. Schematic illustration of the distribution of hydrostatic pressures near a void at the extrusion weld seam.

4 Conclusions

In this research, a special extrusion-welding tooling setup and a sandwich billet configuration were designed to simulate the solid-state bonding occurring inside the porthole die during extrusion in order to reveal atomic diffusion across the solid-state bonding interface. FE simulations of extrusion welding were carried out to calculate the state variables and to aid in analyzing the extrusion-welding phenomena. The atomic diffusion during extrusion welding was confirmed through the model study and the operating mechanisms of atomic diffusion during extrusion welding were clarified. The following conclusions were drawn.

(1) With the designed extrusion-welding tooling setup and sandwich-structured billet configuration, pure magnesium and the Mg-Al-Zn-RE alloy could be symmetrically deformed and extrusion-welded. By means of EPMA and FE simulations, atomic diffusion in the extrusion-welding region could be clearly revealed.

(2) Atomic diffusion indeed occurred across the extrusion weld seam between pure magnesium and the Mg-Al-Zn-RE alloy during extrusion welding. The extent of atomic diffusion could be significantly enhanced by raising billet temperature. The characteristic diffusion length of aluminum into pure magnesium reached 10.2 ± 0.3 μm at a billet temperature of 400 °C (673 K) and stem speed of 0.2 mm/s, which was much greater that the diffusion length when only the concentration gradient was considered.

(3) In addition to the concentration gradient as the driving force, the gradients of stress and hydrostatic pressure also promoted atomic diffusion across the interface during extrusion welding.

Acknowledgments

Conflict of Interest Statement

On behalf of all authors, the corresponding author states that there is no conflict of interest.

References

[1] F. Guo, B. Feng, S. Fu, Y. Xin, S. Xu and Q. Liu: J. Magnes. Alloy., 2017, vol. 5, pp. 13-19. https://doi.org/10.1016/j.jma.2016.12.001.

[2] Y.D. Sun, Q.R. Chen and W.J. Sun: Int. J. of Adv. Manuf. Technol., 2015, vol. 80, pp. 495-506. https://doi.org/10.1007/s00170-015-7030-5.

[3] Z. Liu, L. Li, J. Yi, S. Li and G. Wang: Int. J. of Adv. Manuf. Technol., 2017, vol. 92, pp. 1039-52. https://doi.org/10.1007/s00170-017-0200-x.

[4] D.R. Cooper and J.M. Allwood: J. Mater. Process. Technol., 2014, vol. 214, pp. 2576-92. https://doi.org/10.1016/j.jmatprotec.2014.04.018.

[5] N.F. Kazakov: Diffusion Bonding of Materials, Pergamon Press, Oxford, 1985.

[6] F. Wu, W. Zhou, Y. Han, X. Fu, Y. Xu and H. Hou: Materials (Basel), 2018, vol. 11. https://doi.org/10.3390/ma11081446.

[7] S. Shimizu, H.T. Fujii, Y.S. Sato, H. Kokawa, M.R. Sriraman and S.S. Babu: Acta Mater., 2014, vol. 74, pp. 234-43. https://doi.org/10.1016/j.actamat.2014.04.043.

[8] K.-i. Mori, N. Bay, L. Fratini, F. Micari and A.E. Tekkaya: CIRP Annals, 2013, vol. 62, pp. 673-94. https://doi.org/10.1016/j.cirp.2013.05.004.

[9] B. Xie, M. Sun, B. Xu, C. Wang, D. Li and Y. Li: Mater. Des., 2018, vol. 157, pp. 437-46. https://doi.org/10.1016/j.matdes.2018.08.003.

[10] J. Yu and G. Zhao: Mater. Charact., 2018, vol. 138, pp. 56-66. https://doi.org/10.1016/j.matchar.2018.01.052.

[11] H.Y. Chen, J. Cao, X.G. Song and J.C. Feng: Appl. Phys. Lett., 2012, vol. 100. https://doi.org/10.1063/1.4721665.

[12] A. Hill and E.R. Wallach: Acta Metall., 1989, vol. 37, pp. 2425-37. https://doi.org/10.1016/0001-6160(89)90040-0.

[13] S.-W. Bai, G. Fang and J. Zhou: J. Mater. Process. Technol., 2017, vol. 250, pp. 109-20. https://doi.org/10.1016/j.jmatprotec.2017.07.012.

[14] W. Liu, L. Long, Y. Ma and L. Wu: J. Alloy. Compd., 2015, vol. 643, pp. 34-9. https://doi.org/10.1016/j.jallcom.2015.04.116.

[15] Z. Zhu, R. Shi, A.D. Klarner, A.A. Luo and Y. Chen: J. Magnes. Alloy., 2020, vol. 8, pp. 578-86. https://doi.org/10.1016/j.jma.2020.03.004.

[16] Y. Chen, S. Liu, Y. Zhao, Q. Liu, L. Zhu, X. Song, Y. Zhang and J. Hao: Vacuum, 2017, vol. 143, pp. 150-7. https://doi.org/10.1016/j.vacuum.2017.06.004.

[17] C.Y. Sun, L. Li, M.W. Fu and Q.J. Zhou: Mater. Des., 2016, vol. 94, pp. 433-43. https://doi.org/10.1016/j.matdes.2016.01.058.

[18] J. Tang, L. Chen, G. Zhao, C. Zhang and L. Sun: J. Magnes. Alloy., 2020, vol. 8, pp. 654-66. https://doi.org/10.1016/j.jma.2020.02.016.

[19] C. Zhang, M.Q. Li and H. Li: J. Mater. Sci. Technol., 2018, vol. 34, pp. 1449-54. https://doi.org/10.1016/j.jmst.2017.12.001.

[20] J. Yu, G. Zhao and L. Chen: J. Mater. Process. Technol., 2016, vol. 237, pp. 31-47. https://doi.org/10.1016/j.jmatprotec.2016.05.024.

[21] S.-W. Bai, G. Fang and J. Zhou: Metall. Mater. Trans. A, 2019, vol. 50, pp. 3246-64. https://doi.org/10.1007/s11661-019-05242-9.

[22] O. Sabokpa, A. Zarei-Hanzaki and H.R. Abedi: Mater. Sci. Eng. A, 2012, vol. 550, pp. 31-8. https://doi.org/10.1016/j.msea.2012.03.112.

[23] L. Li, H. Zhang, J. Zhou, J. Duszczyk, G.Y. Li and Z.H. Zhong: Mater. Des., 2008, vol. 29, pp. 1190-8. https://doi.org/10.1016/j.matdes.2007.05.003.

[24] H. Mirzadeh: Mater. Chem. Phys., 2015, vol. 152, pp.123-126. https://doi.org/10.1016/j.matchemphys.2014.12.023.

[25] H. Mehrer: Diffusion in solids: fundamentals, methods, materials, diffusion-controlled processes, Springer Science & Business Media, 2007. https://doi.org/10.1007/978-3-540-71488-0.

[26] W. Zhong and J.-C. Zhao: Scripta Mater., 2017, vol. 127, pp. 92-6. https://doi.org/10.1016/j.scriptamat.2016.09.008.

[27] L. Li, J. Zhou and J. Duszczyk: J. Mater. Process. Technol., 2006, vol. 172, pp. 372-80. https://doi.org/10.1016/j.jmatprotec.2005.09.021.

[28] C.Y. Sun, Y.P. Cong, Q.D. Zhang, M.W. Fu and L. Li: J. Mater. Process. Technol., 2018, vol. 253, pp. 99-108. https://doi.org/10.1016/j.jmatprotec.2017.10.045.

[29] F. Dobeš and P. Dymáček: J. Magnes. Alloy., 2020, vol. 8, pp. 414-20. https://doi.org/10.1016/j.jma.2020.03.001.

[30] C.C. Kammerer, N.S. Kulkarni, R.J. Warmack and Y.H. Sohn: J. Alloy. Compd., 2014, vol. 617, pp. 968-74. https://doi.org/10.1016/j.jallcom.2014.07.193.

[31] Y. Wang, X. Li, D. Dou, L. Shen and J. Gong: Int. J. Hydrog. Energy., 2016, vol. 41, pp. 6053-63. https://doi.org/10.1016/j.ijhydene.2016.03.003.